

A discrete regenerative fuel cell mediated by ammonia for renewable energy conversion and storage

Zhefei Pan^a, Yun Liu^a, Abdullah Tahir^a, Oladapo Christopher Esan^a, Jie Zhu^{b,*}, Rong Chen^{c,d,*}, Liang An^{a,*}

^a Department of Mechanical Engineering, The Hong Kong Polytechnic University, Hung Hom, Kowloon, Hong Kong SAR, China

^b School of Physics Science and Engineering, Tongji University, Shanghai 200092, China

^c Key Laboratory of Low-grade Energy Utilization Technologies and Systems (Chongqing University), Ministry of Education, Chongqing 400030, China

^d Institute of Engineering Thermophysics, Chongqing University, Chongqing 400030, China

*Corresponding authors.

Email: jiezhu@tongji.edu.cn (Jie Zhu)

Email: rchen@cqu.edu.cn (Rong Chen)

Email: liang.an@polyu.edu.hk (Liang An)

Abstract

The sustainable nature of renewable energy, with its vast resource potential and reduced costs, has triggered a rapid increase in its direct utilization in a solar/wind-electricity manner. As the installed capacity increases, cost-effective and efficient technologies for renewable energy storage and utilization will be critically important to mitigate the intermittency of the solar and wind resources and maintain stability of the electrical grid. In this work, we demonstrate a discrete regenerative fuel cell, mediated by ammonia, capable of converting and storing intermittent power in an electricity-fuel-electricity approach. During energy storage (electricity to fuel), charging an electrolysis flow cell for ammonia production from nitrogen and water results in a Faradaic efficiency of 2.18% and a rate performance of $15.03 \times 10^{-10} \text{ mol s}^{-1} \text{ cm}^{-2}$

at room temperature, which is one order of magnitude higher than those reported in the open literature. During energy utilization (fuel to electricity), energizing a flow cell with ammonia results in a peak power density of 8.86 mW cm^{-2} at $80 \text{ }^\circ\text{C}$. Hence, a discrete regenerative fuel cell mediated by ammonia for renewable energy storage and utilization is demonstrated, which represents a promising alternative choice for the regenerative fuel cell mediated by hydrogen in terms of storage, transportation, distribution, and dispensation costs, as well as safety issues.

Keywords: Renewable energy; Energy conversion and storage; A discrete regenerative fuel cell mediated by ammonia; Electricity-fuel-electricity approach; Flow cells

1. Introduction

The widespread use of renewable energy, despite its sustainable nature, falling costs, and large resource potential such as solar and wind, is hindered primarily because of its intermittent nature and unreliability [1-3]. A paramount solution to resolve this matter is to advance energy storage and conversion systems towards securing an effective and reliable supply of renewable electricity [4-6]. Hydrogen, as a mediator, can be produced via the water electrolysis by any of the renewable power sources. Thereafter, the hydrogen can be paired with air in fuel cells to generate electricity on demand [7, 8]. Hence, this electricity-fuel-electricity approach is considered as an effective way for the storage and supply of renewable power [9]. Storing hydrogen, the lightest gas, is realized by compression and liquefaction at low temperatures and high pressures (1.3 MPa at -239.96 °C) in industrial [10]. In addition, storing hydrogen for medium- and long-term and transporting hydrogen for long distance demand high up-front costs for building new infrastructures [11]. Alternatively, ammonia, a hydrogen carrier with a high hydrogen content of 17.6 wt. %, can easily be either liquefied at low pressures (0.8 MPa at 20 °C) or dissolved in water for large-scale storage. The long-distance ammonia transport can reliably depend on the established infrastructure [11]. Compared to hydrogen, in terms of energy carrier, ammonia therefore possesses two striking advantages - milder liquefaction conditions which significantly lower storage cost and alleviate safety issues, as well as the established infrastructure which reduces ammonia storage, transportation, distribution, and dispensation costs [11].

In this work, we demonstrate a discrete regenerative fuel cell (RFC) mediated by ammonia capable of storing and utilizing intermittent power in an electricity-fuel-electricity approach. This discrete RFC combining a fuel cell with an electrolyzer is realized through two independent electrochemical flow cells, i.e., an electrolysis cell for energy storage in the form of ammonia (via nitrogen reduction reaction) and a fuel cell for energy conversion in the form of electricity

(via ammonia oxidation reaction). As illustrated in Fig. S1, electrolysis cells use intermittent power to convert nitrogen and water into ammonia, and simultaneously achieve long-term energy storage in the form of ammonia. Then, ammonia is distributed through the established and reliable infrastructure to end users. On demand, fuel cells can generate power via converting chemical energy stored in ammonia directly into electricity, together with the release of nitrogen and water.

Haber-Bosch process typically produces ammonia from nitrogen and hydrogen via a thermochemical conversion. However, to meet the reaction conditions of high pressures and temperatures, 1-2% of the global energy supply is consumed by this process annually. What's worse, 1% of the total CO₂ emission is released to the atmosphere [12]. Photocatalytic ammonia production, a photochemical/electrochemical process driven by solar energy, is a green and sustainable process, but suffers the poor stability of photocatalysts due to severe photocorrosion and the low production rate due to fast recombination of electron-hole pairs [13]. Alternatively, using renewable power, ammonia also can be produced at ambient conditions via electrochemical nitrogen reduction in an electrochemical cell [14], which typically consists of two big half-cells separated by an ion exchange membrane to form an H-shape cell structure, as shown in Fig. S2 (a). Such a bulky cell configuration creates a large barrier for nitrogen delivery and reduction, seriously limiting the ammonia production rate. Besides this, nitrogen has to dissolve in liquid electrolyte by gas bubbling before nitrogen diffusion and reduction could take place, but the extremely low solubility of nitrogen becomes another performance-limiting factor for this emerging technology [15]. We therefore introduce a flow cell structure borrowed from fuel cells into electrochemical cells, creating a compact electrochemical flow cell. Such a design maintains the unique advantages of the fuel cell architecture, while it also increases the flexibility of component design and system optimization, creating enough room for performance improvement, system cost reduction, and

scale-up into an industrial facility [15].

Conventional ammonia utilization is based on combustion related technologies, such as internal combustion engines, however, the energy efficiency is low due to several steps involved in the conversion process [16]. It has been demonstrated that ammonia is an alternative fuel in direct ammonia fuel cells (DAFCs) for power generation [17]. Impressively, chemical energy stored in ammonia can be directly converted into electricity with a potentially high energy efficiency [18-21]. For instance, high-temperature solid oxide fuel cells (SOFCs) fueled by ammonia can function as stationary power plants supplying grid-connected power, likewise, low-temperature DAFCs can release electricity wherever and whenever on demand providing off-grid power [22], as illustrated in Fig. S2 (b). However, we demonstrate that a low-temperature DAFC effectively converts the renewable energy stored in ammonia into electricity, which can meet more application demands than SOFCs.

In summary, a discrete RFC mediated by ammonia for renewable energy storage and conversion using an electricity-fuel-electricity approach is demonstrated. Charging the flow cell, constituted by an Au/C-coated carbon-cloth cathode and a catalyst-free nickel-foam anode unattached by an alkaline anion exchange membrane (AEM), results in a Faradaic efficiency of 2.18% and an ammonia production rate as high as $15.03 \times 10^{-10} \text{ mol s}^{-1} \text{ cm}^{-2}$ at room temperature, which is at least one order of magnitude higher than those reported in the open literature. Moreover, energizing the fuel cell constituted by a PtRu/C-coated carbon anode and a Pd/C-coated carbon paper cathode separated by an alkaline AEM with ammonia, an open-circuit voltage (OCV) of 0.53 V and a peak power density of 8.86 mW cm^{-2} are achieved at 80 °C.

2. Materials and methods

2.1. Fabrication of membrane electrode assemblies

The membrane electrode assembly (MEA) for the electrolysis cell is constituted by a cathode,

a catalyst-free nickel-foam anode, and a AEM. On the other hand, the MEA for the DAFC consists of a pair of electrodes as well as a pre-treated AEM. The details of the MEA preparation can be found in Supplementary information.

2.2. Cell setups and instrumentation

The setup of the electrolysis cell is shown in Fig. 1. Two polytetrafluoroethylene (PTFE) gaskets were added to prevent the leakage. An electrochemical workstation PGSTAT302N (Metrohm Autolab B.V., Netherlands, potential accuracy of $\pm 0.2\%$, current accuracy of $\pm 0.2\%$) was used to control the electrolysis process. Upon charging, 1.0 M KOH was supplied into the anode at 1.0 mL min^{-1} . The nitrogen (purity of $>99.995\%$) was directly fed into the cathode at set flow rates. Although the nitrogen purity is as high as 99.995%, the nitrogen-containing contaminants such as nitrates, nitrites and nitrogen oxides will lead to an unreliable ammonia production rate. To avoid this issue, an alkaline solution (1.0 M KOH) was placed between the nitrogen cylinder and cathode inlet to adsorb these contaminants.

Similarly, the setup of the DAFC is shown in Fig. 2. An Arbin BT2000 (Arbin instrument Inc., USA, accuracy of 0.02%-0.05% full-scale range) monitored the discharging process and polarization curves of this DAFC. Upon discharging, a mixture solution of KOH and ammonia at 4.0 mL min^{-1} was supplied into the anode. The oxygen was directly fed into the cathode from a cylinder at 10.0 standard cubic centimeter per minute (SCCM).

2.3. Ammonia determination

The produced ammonia was determined by the indophenol blue method [23]. 1.0 mL sample solution was mixed with 1.0 mL solution consisting salicylic acid, sodium citrate, and 1.0 M NaOH, 0.5 mL solution of sodium hypochlorite, and 0.1 mL solution of sodium nitroferricyanide dihydrate in sequence. The final solution was maintained for 2 h, then it was tested by a UV-vis spectrometer (Halo DB-20, Dynamica Scientific Ltd., UK, wavelength accuracy of $\pm 0.3 \text{ nm}$, photometry accuracy of $\pm 0.002 \text{ Abs}$). The calibration curves are shown

in Fig. S3.

3. Results and discussion

3.1. Ammonia production via nitrogen reduction

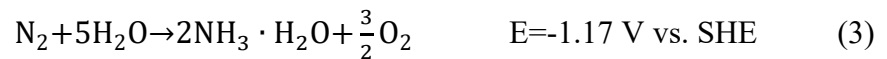
With the applied voltage in our electrolysis cell, the oxygen evolution reaction (OER) happens on the anode, where OH^- is oxidized to oxygen, water, as well as electrons [24]:



The produced electrons are transported through the external circuit from the anode to the cathode. Nitrogen in the cathode receives the arriving electrons and water crossover from the anode, thereby participating in the nitrogen reduction reaction (NRR) to produce ammonia as shown in the following equation [25]:



The internal ionic circuit is formed by the OH^- transporting from the cathode to anode. Thus, the overall reaction is:



3.2. Ammonia production performance

It is indicated in Fig. 3 that the current performance of electrochemical ammonia production is still far lower than the targets proposed by the U.S. Department of Energy (DOE), which are a current density of 300 mA cm^{-2} , a faradaic efficiency of 90%, an ammonia yield of $10^{-6} \text{ mol s}^{-1} \text{ cm}^{-2}$, a degradation rate of 0.3% for 1000 hours, and an energy efficiency of 60% [12, 26].

Due to the H-shape cell with a bulky structure being widely adopted, the applied current densities in previous works are generally single digits, even lower than 1.0 mA cm^{-2} , which is attributed to the huge distance between electrodes, and thus resulting in a longer transport pathway for charge carriers. To our best knowledge, our proposed electrolysis cell with the compact layer-by-layer structure results in the highest current density of 20.0 mA cm^{-2} , which is higher than those reported in the open literature by one or two orders of magnitude, leading

to an ammonia production rate of $15.03 \times 10^{-10} \text{ mol s}^{-1} \text{ cm}^{-2}$. The ammonia production rate per area is evaluated by the active area of MEA, e.g., 4 cm^2 in this work. This value is at least one order of magnitude higher than those reported in the open literature, as shown in Table S1. The ammonia production rates in the aqueous electrolyte in the open literature are generally lower than $3.0 \times 10^{-10} \text{ mol s}^{-1} \text{ cm}^{-2}$, which is attributed to their low applied current densities [27-36]. To improve the production rate, the flow cells employing the molten salt electrolyte operated from 200°C to 500°C have been investigated [37]. The liquid molten salts can dissolve and transfer the reactants to the electrode surface easier than the aqueous electrolyte, contributing to a high ammonia production rate ranging from $1.8 \times 10^{-10} \text{ mol s}^{-1} \text{ cm}^{-2}$ to $200.0 \times 10^{-10} \text{ mol s}^{-1} \text{ cm}^{-2}$ [37]. The Faradaic efficiency, another important target, achieved by our electrolysis cell is 2.18%. Although it is lower than the results of some studies using H-shape cells (1.15% to 32.0%), the current density achieved by our electrolysis cell is much higher, approaching closer to the DOE's target (300 mA cm^{-2}). In addition, comparing with other works using flow cells (0.15% and 0.21%), the Faradaic efficiency achieved in this work is still higher, even when our electrolysis cell is operated at a higher rate. In the flow cells employing the molten salt electrolyte, benefiting from the absence of H_2O , the side reaction of hydrogen evolution reaction (HER) can be largely retarded in molten salts, resulting in greatly enhanced Faradaic efficiency for ammonia production ranging from 4.8% to 80.0% [37]. To improve the Faradaic efficiency, it is crucial to develop novel catalysts to suppress the side reaction of HER. In addition, the cathode is not immersed and saturated by water in flow cells, as nitrogen gas is constantly fed into the flow cell. Hence, the electrode structural design can be an additional method to improve the Faradaic efficiency. For example, in a previous study [38], a high ammonia yield rate of $9.9 \times 10^{-10} \text{ mol cm}^{-2} \text{ s}^{-1}$, a faradaic efficiency of 64.8%, and a specific energy efficiency of 40.7% were achieved by optimizing the electrode design parameters and creating more triple-phase boundaries. Table S1 summarizes the performance comparison of

our work and previous works in terms of Faradaic efficiency and ammonia yield rate.

The effects of current densities, nitrogen flow rates, and cathode catalyst loadings are comprehensively studied, as these critical parameters significantly affect ammonia production performance. Upon charging, the applied current supplies the required electrons to participate in the NRR. It is shown in Fig. 4 (a) that the ammonia yield rate increases from 9.02×10^{-10} mol s⁻¹ cm⁻² to 15.03×10^{-10} mol s⁻¹ cm⁻² as current density increases from 10 mA cm⁻² to 20 mA cm⁻², which is due to the adequate electron supply which in turn enhances the nitrogen reduction to ammonia. While the current density continuously increases to 50 mA cm⁻², the ammonia yield steadily decreases to 9.40×10^{-10} mol s⁻¹ cm⁻², due to the more intense side reaction of HER [23]. Although the ammonia yield is attractive, it should also be mentioned that the Faradaic efficiency is not promising, as it decreases with higher current densities from 2.61% to 0.54%, resulting in a contradiction between the required industrial current density of 300 mA cm⁻² and the high faradaic efficiency of 90%. To address this discrepancy, the development of catalytic materials with satisfactory NRR activity as well as NRR selectivity is of paramount importance [39]. The voltage behavior of this electrolysis flow cell as shown in Fig. S4 (a) is stabilized at all current densities, and the stable voltage increases with current density due to the enlarged internal resistance.

Another reactant of nitrogen is supplied by a nitrogen gas flow, making the gas flow rate an important parameter. It is seen from Fig. 4 (b) that the ammonia yield rate increases from 7.34×10^{-10} mol s⁻¹ cm⁻² to 15.03×10^{-10} mol s⁻¹ cm⁻² as nitrogen flow rate increases from 5 SCCM to 50 SCCM, which is attributed to sufficient nitrogen supply producing more ammonia. While the flow rate further increases to 100 SCCM, it does not contribute to higher ammonia yield rate as expected. On the contrary, the yield rate decreases to 11.18×10^{-10} mol s⁻¹ cm⁻². This phenomenon may be ascribed to two reasons. One is that the water in the humidified nitrogen gas will be more easily accumulated in the cathode because when the flow rate is higher more

water is produced, and thus the HER becomes more severe. The other is that the adsorption and activation of nitrogen molecular on the catalyst is a crucial process in NRR. Once the retention time of nitrogen molecular in the cathode catalyst layer decreases when the flow rate is high, the adsorption and activation of nitrogen molecular will be less feasible, obstructing the following hydrogenation reactions and reducing the ammonia production performance [40]. As the current density is kept at 20 mA cm^{-2} , the Faradaic efficiency first increases from 1.06% to 2.18% and later decreases to 1.62%, showing the same trend with ammonia yield rate. The voltage behavior of this electrolysis flow cell is shown in Fig. S4 (b), and it can be seen that the voltages are stabilized at all nitrogen flow rates, while the cell running at a flow rate of 50 SCCM requires the lowest applied voltage. This is because the necessary reactants (nitrogen and water) are insufficient, when either low nitrogen flow rate of 5 SCCM or high nitrogen flow rate of 50 SCCM is fed into the cell, leading to the severe concentration polarization, and thus an enhanced cathode overpotential.

Ammonia is produced via NRR on the cathode catalyst layer, so the catalyst loading will substantially affect the ammonia yield rate for a given catalyst. It is shown in Fig. 4 (c) that the ammonia yield rate increases from $10.47 \times 10^{-10} \text{ mol s}^{-1} \text{ cm}^{-2}$ to $15.03 \times 10^{-10} \text{ mol s}^{-1} \text{ cm}^{-2}$ with the increase of cathode catalyst loading from 1.0 mg cm^{-2} to 2.0 mg cm^{-2} . The morphologies of these three cathodes are shown in Fig. S5. It is found that the carbon fiber is partially covered by catalyst when the loadings are 1.0 mg cm^{-2} and 1.5 mg cm^{-2} , while the carbon fiber is fully covered by catalyst at the loading of 2.0 mg cm^{-2} , forming more active sites for ammonia production and promoting the ammonia yield rate. Similarly, the Faradaic efficiency increases from 1.51% to 2.18%, sharing the same trend with ammonia yield rate.

3.3. Power generation via ammonia oxidation

Although high-temperature SOFCs using ammonia as fuel owns advantages of high efficiency and power output due to enhanced reaction kinetics. Beyond this, low-temperature DAFCs can

release electricity wherever and whenever on demand, thus meeting application demands in which SOFCs are not suitable for [41]. The anolyte containing ammonia and KOH is supplied into the anode at a constant flow rate. The ammonia oxidation reaction (AOR) takes place on the anode, producing electrons, nitrogen, and water as shown below [42]:



The produced electrons are transported through the external circuit from the anode to the cathode. Oxygen fed into the cathode combines with the electrons and water coming from the anode to participate in the oxygen reduction reaction (ORR) and produce hydroxide ions as shown in the following equation [43]:



The internal ionic circuit is formed by the OH^- transporting from the cathode to anode. Hence, the overall reaction of this fuel cell is as follows:



It is indicated in Fig. 5 that OCV and peak power density achieved by our DAFCs at 80 °C are comparable to those reported in the open literature, as summarized in Table S2 [44]. It should be mentioned that Professor Yushan Yan's group at The University of Delaware has recently demonstrated a DAFC exhibiting a peak power density of 135 mW cm^{-2} at 80 °C, and Professor Gang Wu's group at University at Buffalo, The State University of New York has recently improved the power density to 314 mW cm^{-2} by PtIrZn/CeO₂-ZIF-8 catalyst, indicating that the performance of low-temperature DAFCs has been considerably improved [45, 46].

3.4. Power generation performance

Fig. 5 depicts the polarization and power density curves of DAFCs with various gas flow rates, anolyte flow rates, operating temperatures, and constant-current discharging behavior. It is seen from Fig. 5 (a) that the highest peak power density of 8.86 mW cm^{-2} is achieved with an oxygen flow rate of 10 SCCM at 80 °C, while a higher oxygen flow rate leads to a lower peak power

density. As water is a necessary reactant at the cathode, the cathode will undergo a severe concentration loss due to the fact that water is quickly swept by higher flow rate and stayed at a shortage state. Since water shortage occurs, the hydration of AEM degrades, leading to a higher internal resistance. As can be seen in Fig. 5 (b), there is an increase in cell performance with increasing feed rate in the intermediate-high current density region, where mass transfer processes become more influential on cell performance. The performance is enhanced up to a flow rate of 4.0 mL min^{-1} due to the improved mass transfer processes, but does not increase further with a flow rate of 6.0 mL min^{-1} . The higher anolyte flow rate will poison the anode catalyst, which refers the N_{ad} species is strongly adsorbed on catalyst active sites, reducing the cell performance. Operating the cell at a temperature higher than $60 \text{ }^\circ\text{C}$ could significantly promote the cell performance as evidenced in Fig. 5 (c). On one hand, increasing the operating temperature could effectively enhance the AOR kinetics, as indicated from the performance lower than $60 \text{ }^\circ\text{C}$ that the polarization curve even could not go through the activation polarization region. On the other hand, the internal resistance is remarkably reduced, which is proved by the maximum current density achieved. In general, the highest round-trip efficiency is 22.2% at 10.0 mA cm^{-2} . At 20.0 mA cm^{-2} when the best ammonia production rate is achieved, the round-trip efficiency decreases to 18.4%. Although these values are lower than that of batteries (generally 80%), the proposed discrete regenerative fuel cell mediated by ammonia is capable of storing the renewable energy for a longer time up to years, while batteries can only store the energy for hours to days due to the self-discharge phenomenon. Fig. 5 (d) demonstrates that the fuel cell can be stably operated over than 10 h, indicating the fuel cell can be a promising candidate for practical applications.

4. Conclusions

In this work, a discrete regenerative fuel cell mediated by ammonia for renewable energy conversion, storage, and utilization in an electricity-fuel-electricity approach is successfully

demonstrated, which is a promising alternative for the RFC mediated by hydrogen in terms of storage transmission, distribution, and dispensation costs, as well as safety issues. Charging the electrolysis flow cell for ammonia production results in a Faradaic efficiency of 2.18% and a rate performance of $15.03 \times 10^{-10} \text{ mol s}^{-1} \text{ cm}^{-2}$ at room temperature, which is at least one order of magnitude higher than those reported in the open literature. Energizing the flow cell with ammonia results in an OCV of 0.53 V and a peak power density of 8.86 mW cm^{-2} at 80 °C. The objective of this work, apart from demonstrating the competence and elegance of this discrete RFC mediated by ammonia, is to pursuit green and sustainable solutions for renewable energy conversion, storage, and utilization, as the renewables have the inherent advantages of being energetically and economically efficient, as well as environmentally friendly. This significant advance opens a window of opportunity for breakthroughs in the development of renewable energy conversion and storage technologies, thereby achieving energy, environmental, and ecological sustainability.

Acknowledgements

This work was supported by a grant from the National Natural Science Foundation of China (No. 52022003).

Author contributions

Conceptualization: Liang An, Rong Chen, Jie Zhu, and Zhefei Pan; Methodology: Liang An, Rong Chen, Jie Zhu, and Zhefei Pan; Investigation: Zhefei Pan, Yun Liu, and Abdullah Tahir; Writing – Original Draft: Zhefei Pan, Abdullah Tahir, and Oladapo Christopher Esan; Writing – Review & Editing: Zhefei Pan, Oladapo Christopher Esan, Jie Zhu, Rong Chen, and Liang An.

References

- [1] Deng K, Feng H, Liu D, Chen L, Zhang Y, Li Q. *Journal of Materials Chemistry A* 2021;9:3961-7.
- [2] Liu Q, Pan Z, Wang E, An L, Sun G. *Energy Storage Materials* 2020;27:478-505.
- [3] Pan Z, Bi Y, An L. *Applied Energy* 2019;250:846-54.
- [4] Jiang H, Wei L, Fan X, Xu J, Shyy W, Zhao T. *Science Bulletin* 2019;64:270-80.
- [5] Gu W, Ma T, Ahmed S, Zhang Y, Peng J. *Energy Conversion and Management* 2020;223:113283.
- [6] Pan ZF, An L, Wen CY. *Applied Energy* 2019;240:473-85.
- [7] Yan X, Lin C, Zheng Z, Chen J, Wei G, Zhang J. *Applied Energy* 2020;258:114073.
- [8] Zhao G, Rui K, Dou SX, Sun W. *Advanced Functional Materials* 2018;28:1803291.
- [9] Pan ZF, Chen R, An L, Li YS. *Journal of Power Sources* 2017;365:430-45.
- [10] Yin L, Ju Y. *Frontiers in Energy* 2020;14:530-44.
- [11] Valera-Medina A, Xiao H, Owen-Jones M, David WIF, Bowen PJ. *Progress in Energy and Combustion Science* 2018;69:63-102.
- [12] Tang C, Qiao S-Z. *Chemical Society Reviews* 2019;48:3166-80.
- [13] Guo C, Ran J, Vasileff A, Qiao S-Z. *Energy & Environmental Science* 2018;11:45-56.
- [14] Yao Y, Wang J, Shahid UB, Gu M, Wang H, Li H, et al. *Electrochemical Energy Reviews* 2020;3:239-70.
- [15] Cui X, Tang C, Zhang Q. *Advanced Energy Materials* 2018;8:1800369.
- [16] Kobayashi H, Hayakawa A, Somarathne KDKunkuma A, Okafor Ekenechukwu C. *Proceedings of the Combustion Institute* 2019;37:109-33.
- [17] Afif A, Radenahmad N, Cheok Q, Shams S, Kim JH, Azad AK. *Renewable and Sustainable Energy Reviews* 2016;60:822-35.
- [18] Pan Z, Huang B, An L. *International Journal of Energy Research* 2019;43:2583-91.
- [19] Gu W, Ma T, Li M, Shen L, Zhang Y. *Applied Energy* 2020;258:114075.

- [20] Pan Z, Bi Y, An L. *Applied Energy* 2020;258:114060.
- [21] Pan Z, Bi Y, An L. *Applied Thermal Engineering* 2019;147:1115-24.
- [22] Yan X, Li H, Lin C, Chen J, Han A, Shen S, et al. *Sustainable Energy & Fuels* 2020;4:772-8.
- [23] Li G, Yu Y, Pan Z, An L. *ACS Applied Energy Materials* 2020;3:6735-42.
- [24] Gong M, Dai H. *Nano Research* 2015;8:23-39.
- [25] Guo X, Du H, Qu F, Li J. *Journal of Materials Chemistry A* 2019;7:3531-43.
- [26] Pan Z, Khalid F, Tahir A, Esan OC, Zhu J, Chen R, et al. *Fundamental Research* 2021.
- [27] Kong J, Lim A, Yoon C, Jang JH, Ham HC, Han J, et al. *ACS Sustainable Chemistry & Engineering* 2017;5:10986-95.
- [28] Huang H, Xia L, Shi X, Asiri AM, Sun X. *Chemical Communications* 2018;54:11427-30.
- [29] Liu Q, Zhang X, Zhang B, Luo Y, Cui G, Xie F, et al. *Nanoscale* 2018;10:14386-9.
- [30] Zhang L, Ji X, Ren X, Luo Y, Shi X, Asiri AM, et al. *ACS Sustainable Chemistry & Engineering* 2018;6:9550-4.
- [31] Wang Z, Gong F, Zhang L, Wang R, Ji L, Liu Q, et al. *Advanced Science* 2019;6:1801182.
- [32] Zhang L, Ji X, Ren X, Ma Y, Shi X, Tian Z, et al. *Advanced Materials* 2018;30:1800191.
- [33] Suryanto BHR, Wang D, Azofra LM, Harb M, Cavallo L, Jalili R, et al. *ACS Energy Letters* 2019;4:430-5.
- [34] Suryanto BHR, Kang CSM, Wang D, Xiao C, Zhou F, Azofra LM, et al. *ACS Energy Letters* 2018;3:1219-24.
- [35] Chen S, Perathoner S, Ampelli C, Mebrahtu C, Su D, Centi G. *Angewandte Chemie International Edition* 2017;56:2699-703.
- [36] Chen S, Perathoner S, Ampelli C, Mebrahtu C, Su D, Centi G. *ACS Sustainable Chemistry & Engineering* 2017;5:7393-400.
- [37] Yang J, Weng W, Xiao W. *Journal of Energy Chemistry* 2020;43:195-207.

- [38] Wei X, Pu M, Jin Y, Wessling M. *ACS Applied Materials & Interfaces* 2021;13:21411-25.
- [39] Chen G-F, Ren S, Zhang L, Cheng H, Luo Y, Zhu K, et al. *Small Methods* 2019;3:1800337.
- [40] Wang C, Gu Y, Wu S, Yu H, Chen S, Su Y, et al. *Environmental Science & Technology* 2020;54:1920-8.
- [41] Pan Z, Zhuang H, Bi Y, An L. *Journal of Power Sources* 2019;437:226944.
- [42] Siddiqui O, Dincer I. *Fuel Cells* 2018;18:379-88.
- [43] Pan ZF, An L, Zhao TS, Tang ZK. *Progress in Energy and Combustion Science* 2018;66:141-75.
- [44] Guo Y, Pan Z, An L. *Journal of Power Sources* 2020;476:228454.
- [45] Zhao Y, Setzler BP, Wang J, Nash J, Wang T, Xu B, et al. *Joule* 2019;3:2472-84.
- [46] Li Y, Pillai HS, Wang T, Hwang S, Zhao Y, Qiao Z, et al. *Energy & Environmental Science* 2021;14:1449-60.

Figure captions

Fig. 1. (a) Working Principle of an electrolysis flow cell for ammonia production; (b) schematic of the electrolysis cell; and (c) setup of the electrolysis cell.

Fig. 2. (a) Working Principle of a fuel cell for ammonia utilization; (b) schematic of the fuel cell; and (c) setup of the fuel cell.

Fig. 3. Electrochemical NRR performance comparison. (a) Ammonia production rate; and (b) Faradaic efficiency. (Details in Table S1)

Fig. 4. Electrochemical NRR performance in the electrolysis flow cell. (a) Effect of current densities; (b) effect of flow rates; and (c) effect of cathode loadings.

Fig. 5. Polarization and power density curves of DAFCs with (a) various gas flow rates, (b) various anolyte flow rates, and (c) various operating temperatures, and (d) constant-current

discharging behaviors of the DAFC.

Figures

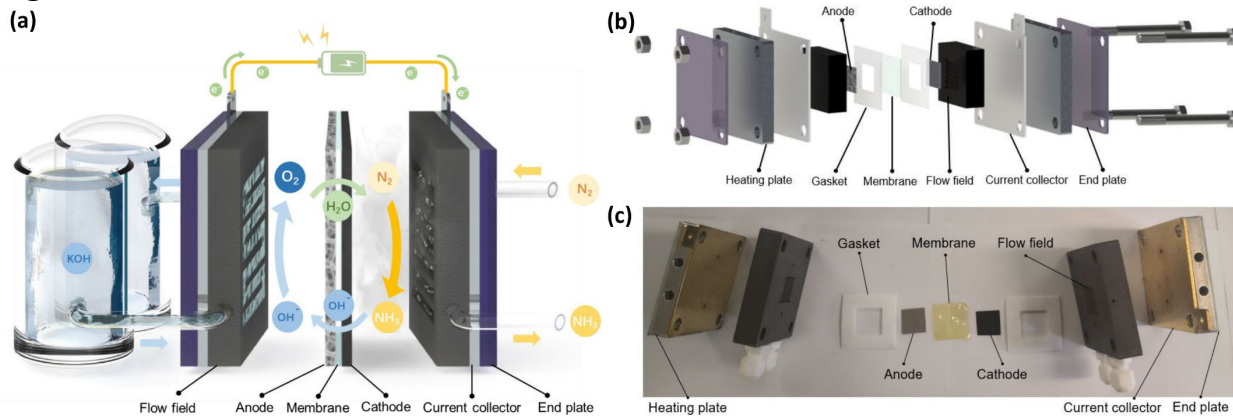


Fig. 1. (a) Working Principle of an electrolysis flow cell for ammonia production; (b) schematic of the electrolysis cell; and (c) setup of the electrolysis cell.

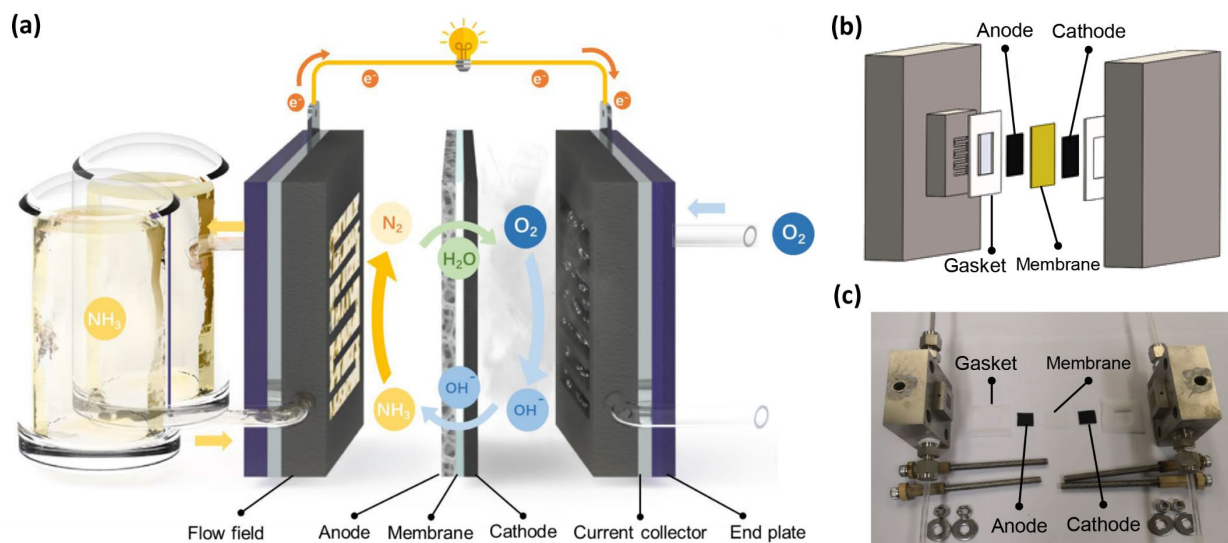


Fig. 2. (a) Working Principle of a fuel cell for ammonia utilization; (b) schematic of the fuel cell; and (c) setup of the fuel cell.

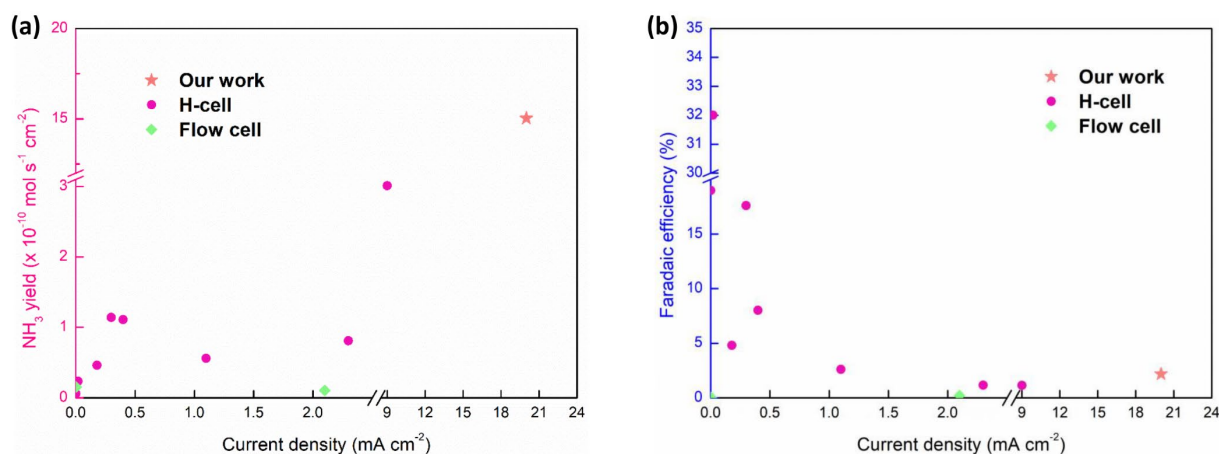


Fig. 3. Electrochemical NRR performance comparison. (a) Ammonia production rate; and (b) Faradaic efficiency. (Details in Table S1)

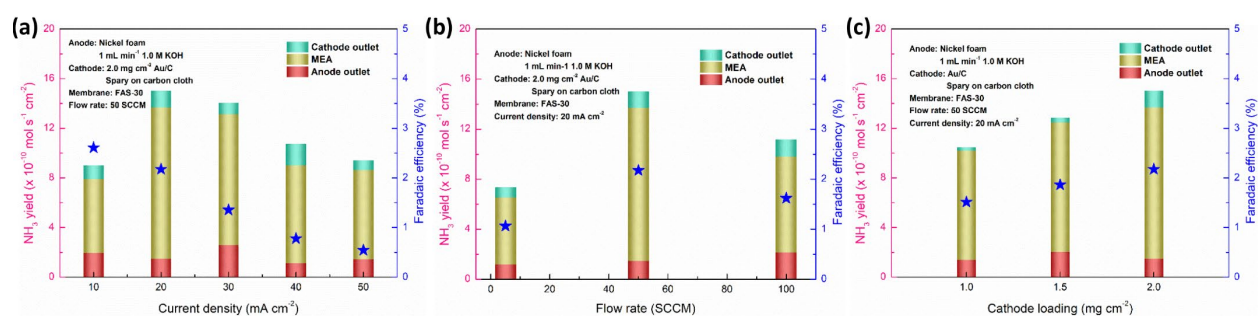


Fig. 4. Electrochemical NRR performance in the electrolysis flow cell. (a) Effect of current densities; (b) effect of flow rates; and (c) effect of cathode loadings.

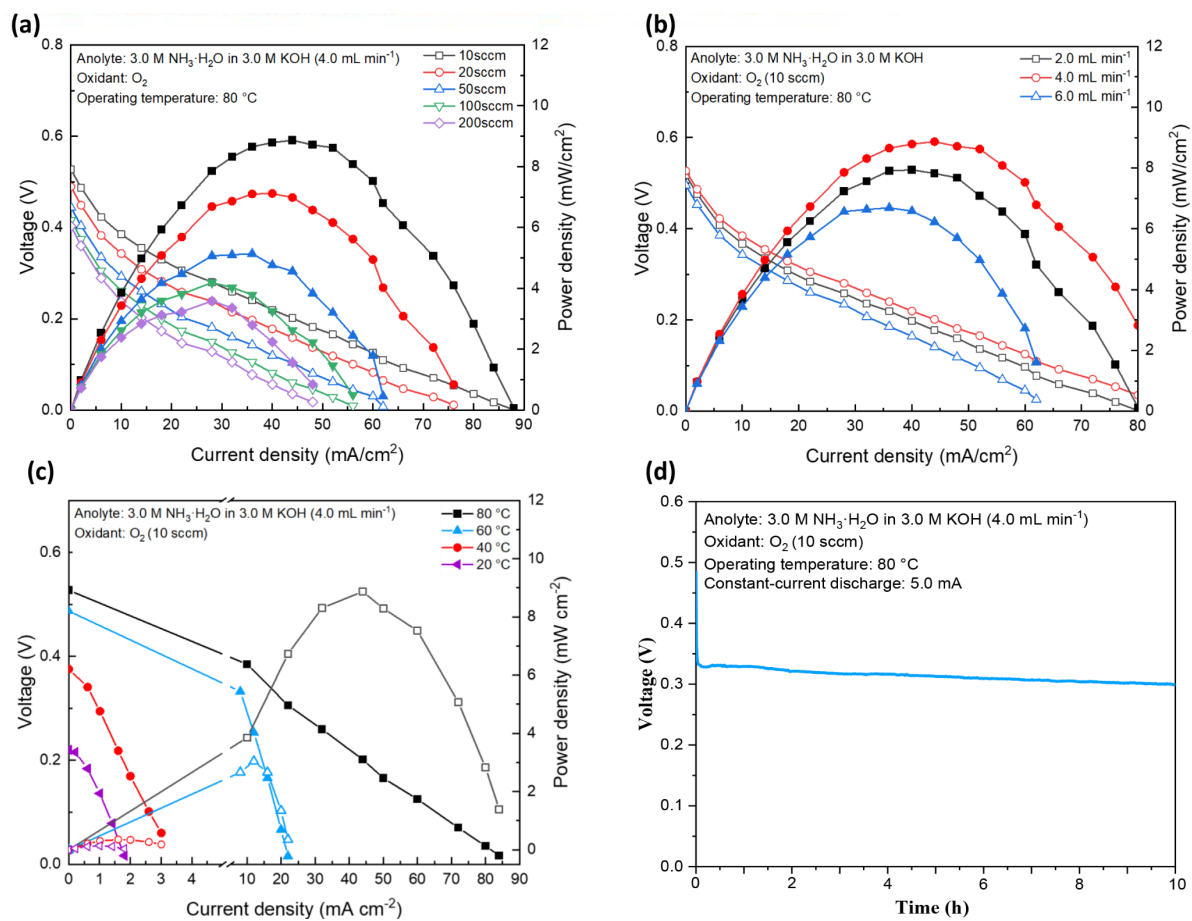


Fig. 5. Polarization and power density curves of DAFCs with (a) various gas flow rates, (b) various anolyte flow rates, and (c) various operating temperatures, and (d) constant-current discharging behaviors of the DAFC.

Supplementary information

A discrete regenerative fuel cell mediated by ammonia for renewable energy conversion and storage

Zhefei Pan^a, Yun Liu^a, Abdullah Tahir^a, Oladapo Christopher Esan^a, Jie Zhu^{b,*}, Rong Chen^{c,d,*}, Liang An^{a,e,*}

^a Department of Mechanical Engineering, The Hong Kong Polytechnic University, Hung Hom, Kowloon, Hong Kong SAR, China

^b School of Physics Science and Engineering, Tongji University, Shanghai 200092, China

^c Key Laboratory of Low-grade Energy Utilization Technologies and Systems (Chongqing University), Ministry of Education, Chongqing 400030, China

^d Institute of Engineering Thermophysics, Chongqing University, Chongqing 400030, China

^e The Hong Kong Polytechnic University Shenzhen Research Institute, Shenzhen 518057, China

*Corresponding authors.

Email: jiezhu@tongji.edu.cn (Jie Zhu)

Email: rchen@cqu.edu.cn (Rong Chen)

Email: liang.an@polyu.edu.hk (Liang An)

1. Methods

1.1. Fabrication of membrane electrode assemblies

The membrane electrode assembly (MEA) for the ammonia production cell consists of a home-made cathode, a bare nickel foam, and a pre-treated anion exchange membrane (AEM). The active area of the electrodes was 2.0 cm × 2.0 cm. The catalyst ink was first obtained via mixing 40 wt.% Au/C (Premetek Co., USA), 5 wt.% Nafion (Fuel Cell Store, USA), and ethanol, which serve as the catalyst, binder, and solvent, respectively. An ultrasonic bath was applied

to the ink for 20 minutes. Subsequently, the ink was sprayed onto the diffusion layer, i.e., carbon paper (Toray, Japan). The desired catalyst loading was obtained by controlling the number of spraying times. To obtain the AEM, original Fumasep FAS-30 membrane in bromide form was cut to the designed area ($3.0 \text{ cm} \times 3.0 \text{ cm}$) and immersed in 1.0 M KOH solution at room temperature for 24 h to transfer them in hydroxide form.

The MEA for the power generation cell consists of a pair of electrodes as well as a pre-treated AEM. The active area of electrodes was $1.0 \text{ cm} \times 1.0 \text{ cm}$. The anode is a commercial electrode with PtRu/C as the catalyst (Pt:Ru=1:1, loading of 4.5 mg cm^{-2}) and carbon paper as the substrate (Johnson Matthey, UK). The conventional dual-layer cathode was fabricated by spraying method. The catalyst ink was first prepared via mixing 10 wt.% Pd/C (Sigma Aldrich, USA), 10 wt.% Nafion (Fuel Cell Store, USA), and ethanol, which serve as the catalyst, binder, and solvent, respectively. An ultrasonic bath was also applied to the ink for 20 minutes. For spraying, ink was sprayed onto the diffusion layer, i.e., carbon paper (Toray, Japan) until the required catalyst loading, $0.55 \text{ mg}_{\text{Pd}} \text{ cm}^{-2}$, was attained. The AEM is obtained by treating the Fumasep FAS-30 membrane with designed area ($2.0 \text{ cm} \times 2.0 \text{ cm}$) in 1.0 M KOH solution at room temperature for 24 h.

1.2. Collection of ammonia

To get rid of nitrogen-containing contaminants, an alkaline solution (1.0 M KOH) was placed between the nitrogen cylinder and cathode inlet to adsorb these contaminants. Ammonia is originally produced on the cathode catalyst layer, and transported to the cathode outlet with nitrogen flow as well as anode outlet derived from ammonia crossover referring to ammonia transporting from cathode through AEM to anode. Therefore, to collect the produced ammonia precisely, an acid trap (H_2SO_4 solution, $\text{pH} = 3.0$) was placed at the cathode outlet to collect the ammonia in the exhausted nitrogen flow, the outflow anolyte was stored in a flask to collect

the crossovered ammonia in the anolyte, and the MEA was dipped in 1.0 M KOH solution for 24 h to collect the ammonia remained in the MEA.

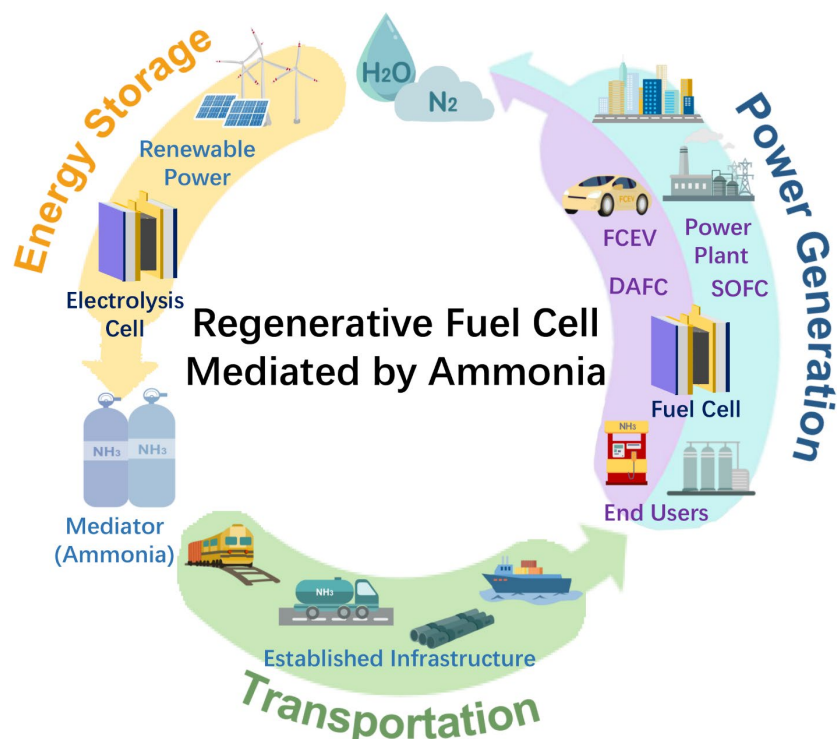


Fig. S1. Illustration of a discrete regenerative fuel cell mediated by ammonia.

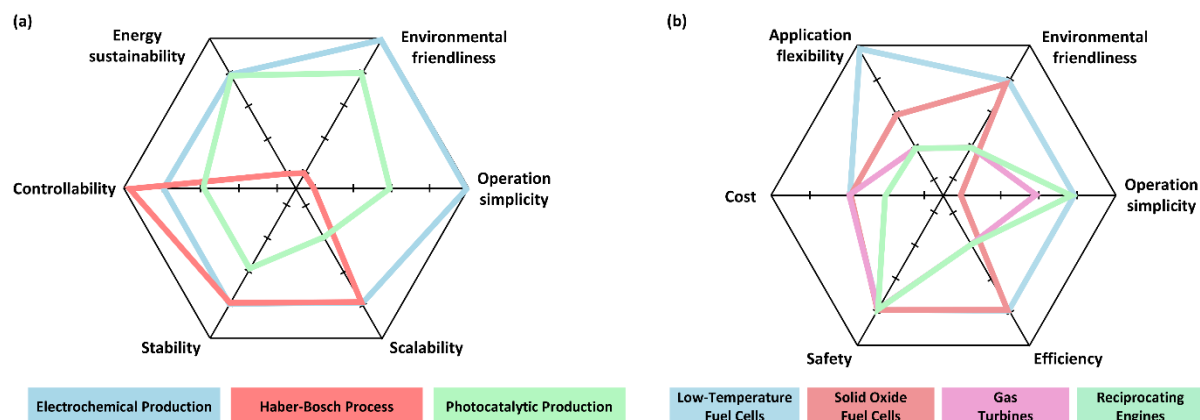


Fig. S2. (a) Comparison among various nitrogen fixation processes (electrochemical production, Haber-Bosch process, and photocatalytic production); and (b) comparison among various ammonia utilization processes (low-temperature fuel cells, solid oxide fuel cells, gas turbines and reciprocating engines).

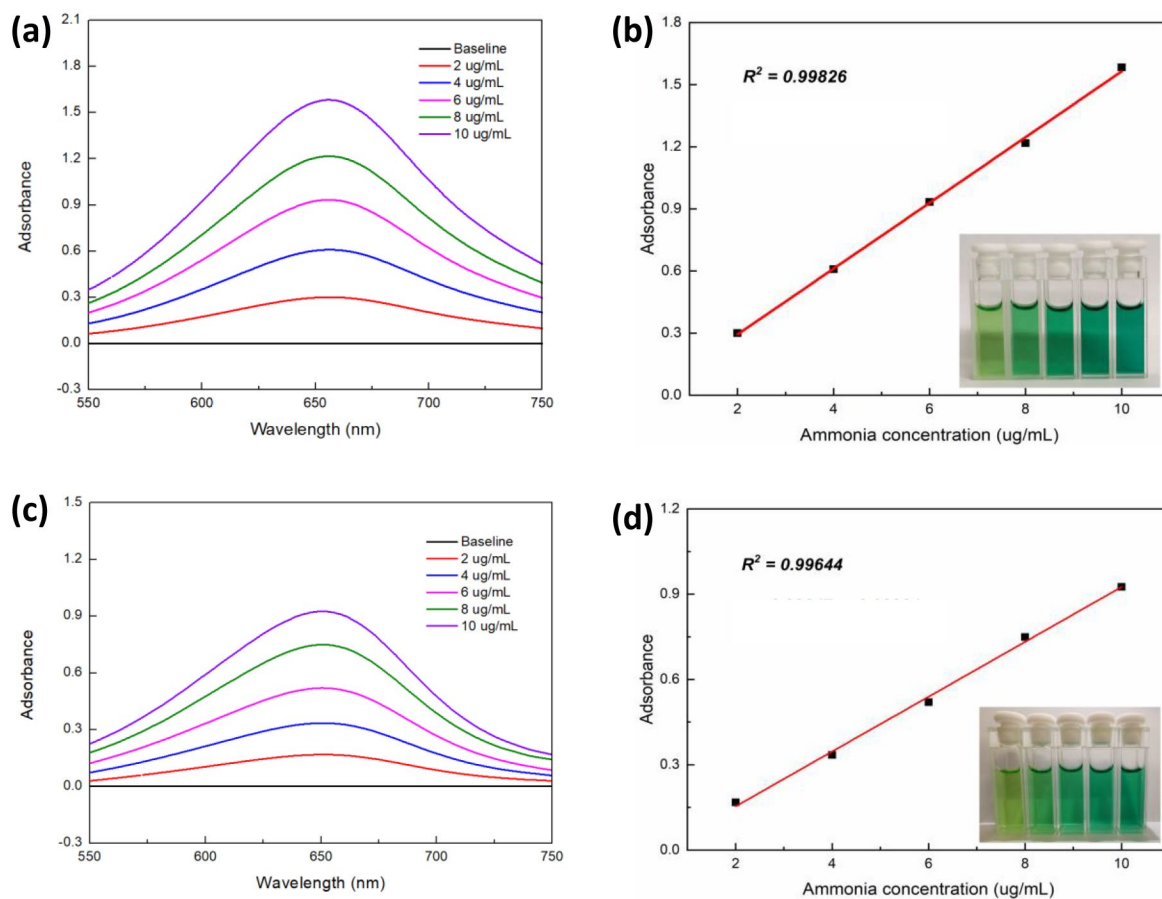


Fig. S3. (a) UV-vis adsorption spectra and (b) calibration curve at acid condition. (c) UV-vis adsorption spectra and (d) calibration curve at alkaline condition.

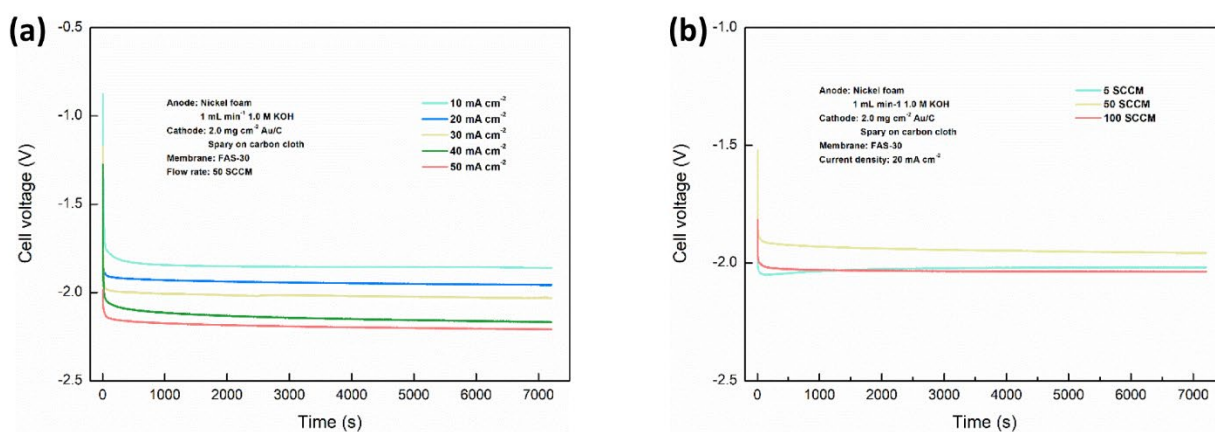


Fig. S4. Effects of (a) current density and (b) nitrogen flow rate on the voltage behavior of the electrolysis flow cell.

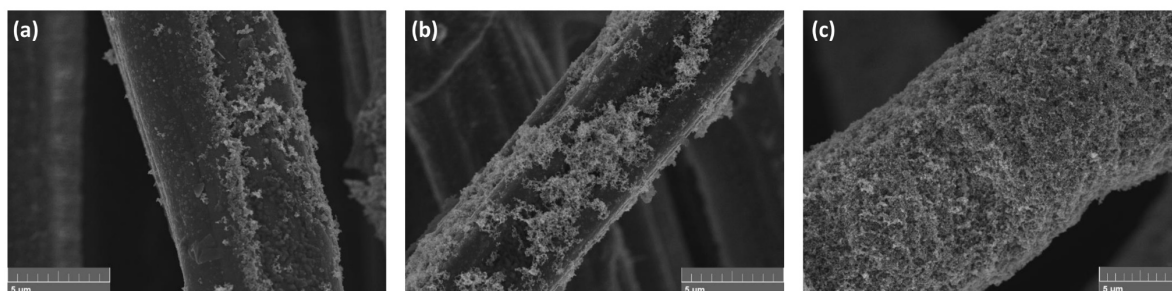


Fig. S5. SEM images of home-made cathode for ammonia production with different loadings. (a) 1.0 mg cm^{-2} , (b) 1.5 mg cm^{-2} , and (c) 2.0 mg cm^{-2} .

Current density (mA cm^{-2})	NH_3 yield ($\times 10^{-10} \text{ mol s}^{-1} \text{ cm}^{-2}$)	Faradaic efficiency (%)	Journal	Reference
0.0015	0.06	2.18	ACS Sustainable Chemistry & Engineering	[1]
0.18	0.46	4.8	Chemical Communications	[2]
1.1	0.56	2.6	Nanoscale	[3]
9.0	3.01	1.15	ACS Sustainable Chemistry & Engineering	[4]
0.4	1.11	8.02	Advanced Science	[5]
2.3	0.81	1.17	Advanced Materials	[6]
0.3	1.14	17.6	ACS Energy Letters	[7]
0.02	0.24	32	ACS Energy Letters	[8]
0.05	0.004	0.15	Angewandte Chemie International Edition	[9]
2.1	0.11	0.21	ACS Sustainable Chemistry & Engineering	[10]
20.0	15.03	2.18		Our work

Table S1. Performance comparison among various electrochemical cells for ammonia production.

Temperature ($^{\circ}\text{C}$)	OCV (V)	Peak power density (mW cm^{-2})	Journal	Reference
80	0.63	135	Joule	[11]
50	0.54	~ 3.07	Journal of Power Sources	[12]
50	0.40	~ 4.15	Electrochimica Acta	[13]
40	0.41	1.32	International Journal of Hydrogen Energy	[14]
40	0.29	0.52	Applied Catalysis A: General	[15]
80	0.53	8.86		Our work

Table S2. DAFC performance comparison.

References

1. J. Kong, A. Lim, C. Yoon, J. H. Jang, H. C. Ham, J. Han, S. Nam, D. Kim, Y.-E. Sung, J. Choi and H. S. Park, *ACS Sustainable Chem. Eng.*, 2017, **5**, 10986-10995.
2. H. Huang, L. Xia, X. Shi, A. M. Asiri and X. Sun, *Chem. Commun.*, 2018, **54**, 11427-11430.
3. Q. Liu, X. Zhang, B. Zhang, Y. Luo, G. Cui, F. Xie and X. Sun, *Nanoscale*, 2018, **10**, 14386-14389.
4. L. Zhang, X. Ji, X. Ren, Y. Luo, X. Shi, A. M. Asiri, B. Zheng and X. Sun, *ACS Sustainable Chem. Eng.*, 2018, **6**, 9550-9554.
5. Z. Wang, F. Gong, L. Zhang, R. Wang, L. Ji, Q. Liu, Y. Luo, H. Guo, Y. Li, P. Gao, X. Shi, B. Li, B. Tang and X. Sun, *Adv. Sci.*, 2019, **6**, 1801182.
6. L. Zhang, X. Ji, X. Ren, Y. Ma, X. Shi, Z. Tian, A. M. Asiri, L. Chen, B. Tang and X. Sun, *Adv. Mater.*, 2018, **30**, 1800191.
7. B. H. R. Suryanto, D. Wang, L. M. Azofra, M. Harb, L. Cavallo, R. Jalili, D. R. G. Mitchell, M. Chatti and D. R. MacFarlane, *ACS Energy Lett.*, 2019, **4**, 430-435.
8. B. H. R. Suryanto, C. S. M. Kang, D. Wang, C. Xiao, F. Zhou, L. M. Azofra, L. Cavallo, X. Zhang and D. R. MacFarlane, *ACS Energy Lett.*, 2018, **3**, 1219-1224.
9. S. Chen, S. Perathoner, C. Ampelli, C. Mebrahtu, D. Su and G. Centi, *Angew. Chem. Int. Ed.*, 2017, **56**, 2699-2703.
10. S. Chen, S. Perathoner, C. Ampelli, C. Mebrahtu, D. Su and G. Centi, *ACS Sustainable Chem. Eng.*, 2017, **5**, 7393-7400.
11. Y. Zhao, B. P. Setzler, J. Wang, J. Nash, T. Wang, B. Xu and Y. Yan, *Joule*, 2019, **3**, 2472-2484.
12. S. Suzuki, H. Muroyama, T. Matsui and K. Eguchi, *J. Power Sources*, 2012, **208**, 257-262.
13. T. Okanishi, Y. Katayama, H. Muroyama, T. Matsui and K. Eguchi, *Electrochim. Acta*, 2015, **173**, 364-369.
14. M. H. M. T. Assumpção, S. G. da Silva, R. F. B. de Souza, G. S. Buzzo, E. V. Spinacé, A. O. Neto and J. C. M. Silva, *Int. J. Hydrogen Energy*, 2014, **39**, 5148-5152.
15. J. C. M. Silva, S. G. da Silva, R. F. B. De Souza, G. S. Buzzo, E. V. Spinacé, A. O. Neto and M. H. M. T. Assumpção, *Appl. Catal., A*, 2015, **490**, 133-138.

Highlights

- A regenerative fuel cell mediated by ammonia is demonstrated.
- It stores and converts renewable energy in an electricity-fuel-electricity way.
- An ammonia production rate of $15.03 \times 10^{-10} \text{ mol s}^{-1} \text{ cm}^{-2}$ is achieved.
- An OCV of 0.53 V and a peak power density of 8.86 mW cm^{-2} are achieved at 80 °C.

